Methodology for stability assessment of discretised shell structures during robotic assembly

Sam Wilcock[1][0000-0002-8353-6219], Mehmet R Dogar[2][0000-0002-6896-5461] and Ornella Iuorio[3][0000-0003-0464-296X]

[1] University of Leeds, UK
s.wilcock@leeds.ac.uk
[2] University of Leeds, UK
[3] Politecnico di Milano, IT

Abstract. Timber structure design can reduce embodied carbon for large span systems, by reducing material usage. The work in this paper presents the assessment of wood panel shell structures, focusing on the use of traditional joinery styles to produce self-supported structures. Key design criteria are to minimise external scaffolding to reduce falsework waste, to allow dry stacking without adhesive between panels for de-construction, and to be manufactured and assembled using digital processes. Focusing on a particular shell geometry, selected for its theoretical performance, a procedure is outlined for the definition of integral joints between planar panels. By modelling deflection using the coupled rigid-block analysis (CRA), different joint styles are assessed during and post-assembly, to compare their suitability and demonstrate the mitigation of falsework. Panels are both 3D printed and built as stacked plywood, validating the utility of CRA and finding the effect of scale to demonstrate its use as a structural design tool for intermediate assembly stages.

Keywords: Shell structures, rigid-block analysis, laser cutting, dry stacking, 3D printing, timber design, assembly sequencing

1 Introduction

The implication of building a form-found shell structure is that it is stable once fully assembled due to a membrane dominant stress profile, but it is not at all guaranteed during assembly, and this usually requires the use of temporary formwork. Computational techniques, such as the coupled rigid-block analysis technique (CRA) have been developed to test stability in block-like structures [1], working on the assumption that discrete elements act as rigid block elements with corresponding interaction forces, moments and friction driving parts to either static equilibrium or collapse. Additionally, the CRA method and its predecessor rigid block equilibrium (RBE) solver [2] have been integrated into ETH's COMPAS software package as COMPAS CRA [3], allowing easy conversion from CAD software Grasshopper's [4] solids and meshes into Python datastructures. Interfaces are found via a similar technique using a geometry package, and then the equilibrium coefficient matrices, friction and load vectors generated

automatically. Displacements are additionally estimated by the coupling of the rigid block equations with kinematics.

The authors of this work study the wider field of robotic assembly of discrete shell structures. To this end, it is useful to be able to understand the stability of intermediate or local assembly stages as well as the global stability. For the sake of reducing material waste, and promoting reusability, it is also beneficial to mitigate formwork requirements traditionally associated with shell construction, and this presents questions about how to design shell panels which can temporarily support bending moments during assembly. Joint design is a key method by which discrete shell structures might be able to support these moments. Assessing specific joints designs for both stability and feasibility of assembly is a problem which must be integrated into the design process.

Feasibility of assembly for translational assemblies is an old computational problem [5]. Datastructures such as non-directional blocking graphs (NDBGs) can be used to describe blocking relationships between parts and can be integrated into design tools to verify the sequence and insertion of neighbouring elements [6].

Whilst the aforementioned CRA method was shown to be accurate at capturing the stability of the Armadillo [7] shell, which is characterised by both concave and convex geometries, it has not been previously exploited to assess the intermediate assembly process of shells or used for its displacement estimation. Therefore, the novelty of this work is to demonstrate CRA use as an early-stage design tool for assessing the stability throughout the assembly process, with a dual inspection of the parallel between stability and the local translational freedom of elements.

2 Methods

2.1 Design of the shell structure surface and discretisation

We propose a shell design that can be assembled using digital manufacturing tools. An initial base surface was designed and turned into a funicular form using the Kangaroo plugin's energy-based approach of minimising strain energy through a mesh. Panelling tools generally require the provision of untrimmed base NURBS surfaces due to how patterns are parameterised, and so by fitting lofts to a series of contour curves a close approximation surface to the shell mesh is obtained. The surface was tiled into hexagons which were then planarized and extruded along local normals at the hexagon corners [8] – in this way the panel edges between neighbours were kept colinear. Comparing to robot manipulator workspace analysis, the structure was checked to be a feasible assembly for a specific robot arm. Through sampling the surface at evenly spaced points at each step of the design, and comparing the distance of points to matching ones on previous surfaces using mean squared error, the relative changes to the design from each step could be quantified:

$$MSE = \frac{\Sigma_{\mathrm{i}=0}^{n} d_i^2}{n} \tag{1}$$

where d_i is the Euclidean distance of the two nearest test points number i between surfaces at two design steps; and n is the number of test points.

2.2 Joint design

The aim of the design was to ensure a locally stable structure, that is, one that could stand unaided during the assembly process. Of some standard woodworking joint styles, dovetails and finger joints were identified as being potentially viable and manufacturable.

Parameterisation of base joints Basic parameterisation of both joint styles were initially created in Grasshopper (see Fig. 1). Joints were defined as planar curves to be extruded through mated panels, with a base line of the curve being drawn between coordinates $(0,0)$ and $(1,0)$ in the XY plane. Due to the use of the curves for extrusion, they were closed to allow boundary surfaces to be created. By allowing for the adjustment of the joint parameters, it would be possible to make comparisons between different percentages of edges covered by joints, as well as estimate the effect on deflection properties. For this work, the dovetail parameters were set as $w = 0.3, \theta = 70°$, whilst the finger joints parameters were set as $w = 0.2, h = 0.12$.

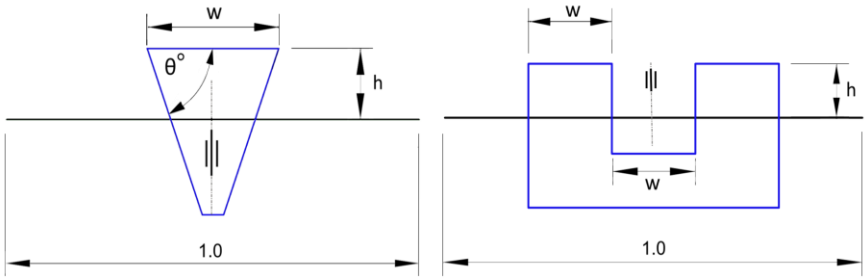

Fig. 1: Parameterisation of the two investigated joint styles, in blue, with vertical lines of symmetry. The reference line in black has length set as 1.0x the length of the edge it will be oriented onto; the *w* and *h* parameters are a percentage of this base length**.**

Calculating panel liaison matrix To reorient the scaled joints throughout the structure, it was required to find the topology of the shell structure. In our previous work on shell assembly sequencing, we demonstrated the use of Rhinoceros®' RhinoCommon method FindCoincidentBrepComponents to deconstruct a list of BREPs into their respective faces and find neighbouring faces within a certain tolerance [6]. Using this, it is possible to compactly describe the connections in an n-panelled structure as a binary $n \times n$ liaison matrix.

For this work, the liaison matrix was extended by additionally comparing panel centroids, and altering the matrix such that neighbours are assigned a +1 or -1 depending on whether they are higher or lower than the test panel (Fig. 2). The modified liaison matrix now allows further components in the definition to apply different rules to neighbours depending on their position relationships, for example, horizontal neighbours could have different joint styles than vertical neighbours to provide changing stiffness depending on whether joints are longitudinal or transverse to the main shell direction. Additionally, since the custom Grasshopper node is already testing for adjacent faces, it is also set to output a DataTree structure containing the face boundaries of these pairs of mating surfaces, without any major additional computing overhead.

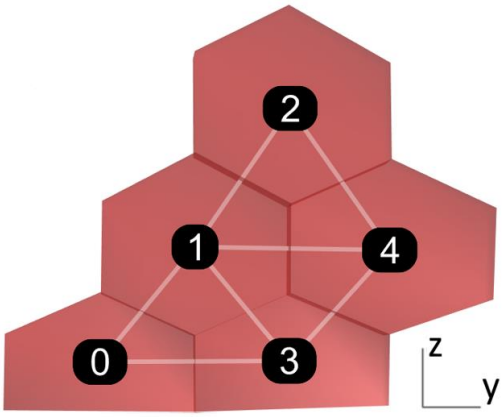

$$L = \begin{bmatrix} \mathbf{0} & \mathbf{1} & \mathbf{0} & \mathbf{0.5} & \mathbf{0} \\ \mathbf{-1} & \mathbf{0} & \mathbf{1} & \mathbf{-1} & \mathbf{0.5} \\ \mathbf{0} & \mathbf{-1} & \mathbf{0} & \mathbf{0} & \mathbf{-1} \\ \mathbf{0.5} & \mathbf{1} & \mathbf{0} & \mathbf{0} & \mathbf{1} \\ \mathbf{0} & \mathbf{0.5} & \mathbf{1} & \mathbf{-1} & \mathbf{0} \end{bmatrix}$$

Fig. 2*:* An example hexagon panel assembly with liaison graph overlay and associated extended liaison matrix. Note that the matrix could be made antisymmetric by encoding horizontal neighbours as +ve or -ve depending on relative y-location.

Propagating joint designs Jiménez described the use of such liaison matrices for understanding precedence constraints in assembly sequencing [9]. In this work, they were applied both for understanding precedence in assembly sequencing and as a tool for deciding where to place sets of joints. Provided the face boundary structure and taking inspiration from Rezaei Rad's exploitation of RhinoCommon's native ChangeBasis Transforms [10], it is possible to take the previously designed joints in the world XY plane and reorient them throughout the structure along neighbouring panel's edges.

The parameterised joint curves were scaled to match the length of each top edge, before being reoriented into the plane of the "male" part that will be inserted into its neighbour. Using the liaison matrix, this is decided by propagating joints only to neighbours with relationships described by a -1 or 0.5, downwards or across. This ensures that each part is inserted male into female from above, implicitly enforcing the precedence requirement that parts are inserted once all lower neighbours are present.

Once the curves were propagated through the panel edges, they were then converted into planar surfaces and extruded through the thickness of the panel. To enable the addition of joint tolerance, scaled copies of each joint were made about centroids, with a scaling factor of $C_{joint} \geq 1.0$, where $C_{joint} = 1.0$ represents a perfect fit and increasing values give greater flexibility in the joint insertion. $C_{joint} = 1.07$ was used throughout.

The extrusion direction for the joints is along the panel conic vectors, meaning that the male surfaces also end up with the same conic shape as their panels and allowing panels to be fitted via translation into multiple slots simultaneously. By taking solid Boolean unions of the panels with the reoriented joint solids, and then taking solid Boolean differences of the panels with the scaled cutting solids, the panels and their integral joints are generated (Fig. 3).

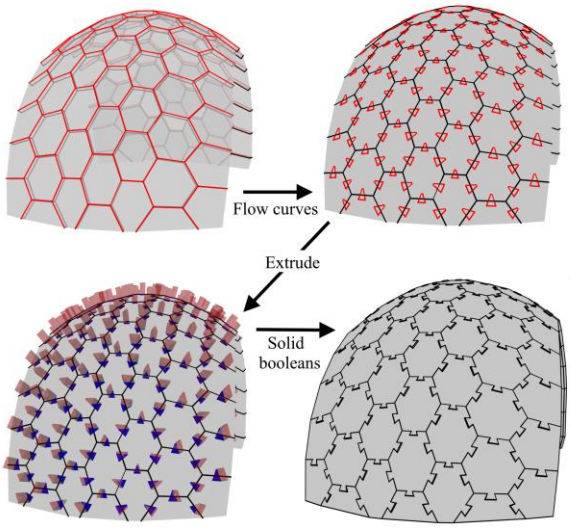

Fig. 3*:* Flowing and extruding joint curves through the shell geometry. First, top edges are found, joint designs are scaled and rotated to match male panel planes. The curves are then extruded (bottom left) with longer, larger red areas indicating cutting solids, blue indicating joints to union.

2.3 Coupled rigid-block analysis and comparison to 3DP model

To validate the CRA method for such discretised shells, a subsection of the full shell was selected for manufacture. Testing was done by comparison of CRA to measurements of the deflected height for the central 3D printed panels (Fig. 4).

By adding a small change to the code for COMPAS CRA, it also became possible to add external forces to the model and thus estimate the effects of additional dead loads on the structure. A custom ghPython component then allows quick export of models to JSON data describing the assembly, which were analysed for stability and displacement at various steps through the assembly process before being passed back to Grasshopper for viewing.

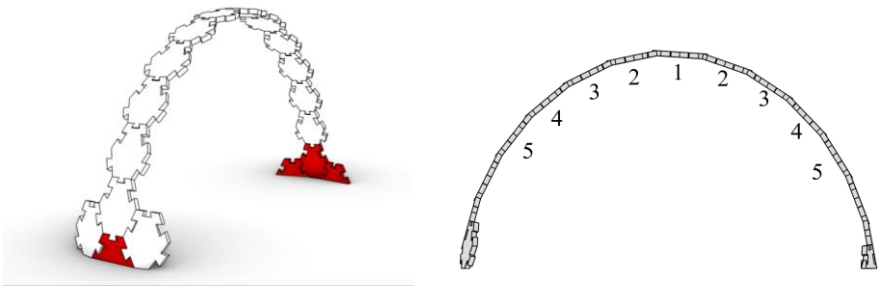

Fig. 4: Left) Subset of panels tested via CRA and through 3D printing. Red panels are those set as fixed base points for CRA modelling. **Right**) Numbered sequence of panels removed during the test.

2.4 Assembly sequencing through non-directional blocking graphs

Assembly sequencing allows a different insight into the assembly, allowing us to find a) if it is possible to assemble the arch using translational movements, and b) a sequence of parts and insertion directions. Previous work detailed the implementation of this process and the components written for Grasshopper [6], and is briefly summarised here.

The normal directions of all the planes comprising an interface surface, for panel i from neighbour j collected into a set, $X_{normal.i,j}$. Additionally, a set of test vectors of unit length, $\mathrm{X_{test}}$, is generated, evenly sampling 3D space through a Fibonacci sphere. By comparing every interface vector with every test vector, the condition for a direction that the panel motion is blocked translationally by a neighbour is:

$$\vec{\mathrm{x}}_{\mathrm{test}} \cdot \vec{\mathrm{x}}_{\mathrm{normal}} > 0 \tag{2}$$

and these matching vectors are added to a set $\mathrm{X_{blocked\ i,j}}$, whilst free directions are the set difference of test vectors and blocked vectors,

$$\mathrm{X_{free\ i,j}} = \mathrm{X_{test}} \backslash \mathrm{X_{blocked\ i,j}}. \tag{3}$$

As panels are added to the structure, further neighbours become blocked, and so assembly sequences and potential free directions of insertion can be found using breadth-first search on the liaison graph and the sets of blocking relationships between panels, recalculating the total set of free panels at each step [11].

3 Results

3.1 Shell design step effects

In Table 1, the different design steps are compared to demonstrate the amount of change that each step introduces to the design surface. Note particularly the order of the mean squared error calculation for the process of fitting a NURBs surface to the form-found mesh.

Table 1. Measured MSE across sampled points between two surfaces.

Test surface A	Test surface B	MSE (m^2)
Catenary mesh	Base surface	2.63×10^{-3}
Fitted loft	Catenary mesh	6.64×10^{-4}
Fitted loft	Base surface	2.45×10^{-3}
Planarized panelled	Catenary mesh	2.42×10^{-2}

3.2 Initial validation of CRA applied to 3DP arch model

There is significant droop in the structure (Table 2), which is most noticeable at case 1, with a maximum drop of 28% at the end point and least visible for the parts closest to

the base. A relatively small sag is exhibited in the fully assembled arch, as would be expected since the arch has support from both ends and is based on a funicular.

Table 2. Comparison of predicted vs measured deflection heights and prediction error for 3DP arch vs. CRA model, with cases from Fig. 4 taking measurements on Left and Right.

#	Design height (mm) h_d		Predicted height (mm) h_P		Measured height (mm) h_m		Difference (mm) $h_m - h_p$		% Deflection $-\frac{h_m - h_d}{h_d}$		Error (%) $\varepsilon = \frac{h_m - h_p}{h_m}$		Average absolute error (%) $\frac{\lvert\varepsilon_L\rvert + \lvert\varepsilon_R\rvert}{2}$
	L	R	L	R	L	R	L	R	L	R	L	R	
0	250	246	241	239	243	240	2	1	3	2	1	0	1
1	250	246	187	201	179	190	-8	-11	28	23	-4	-6	5
2	239	228	198	201	202	194	4	-7	15	15	2	-4	3
3	213	197	190	183	190	179	0	-4	11	9	0	-2	1
4	178	156	165	150	166	148	1	-2	7	5	1	-1	1
5	133	108	129	108	129	105	0	-3	3	3	0	-3	1

The modified CRA Python script with added loads was tested with gradually increasing vertically downward dead loads on the top central panel, ultimately predicting a max load of 823g for a small 3D printed model, spanning 510 mm with a max height of 250 mm and panel thickness 5 mm. This was tested physically, and the structure carried a 590g measuring tape (Fig. 5), however it should be noted that it was precarious and seemed unlikely to take any more mass, as the panels were shifting and pushing outwards towards the base.

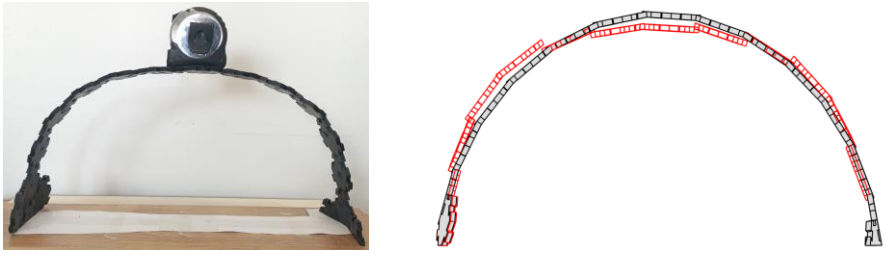

Fig. 5: Dead load testing. **Left)** The shape of the structure can be seen with a mass on the central panel. **Right)** The CRA model of the structure with its ultimate load, where the panels are predicted to separate (original design in black, failure mode in red).

3.3 Comparison of joint styles

Applying the same CRA case study to a finger jointed version, whilst the fully assembled arch was found to be stable as expected due to its funicular nature, only cases 4 and 5 were predicted stable from the set of reduced arches, with the mass of panels in longer cantilevered assemblies causing rotation about the joint interface and failure.

Part freedom testing also provided some differing results between the two joint styles (Fig. 6). The dovetail style is self-constraining, such that at any time, only the

uppermost members without higher neighbours can be removed. On the other hand, for the finger-jointed structure, there is more freedom within the structure at any time – large areas of panels could be removed at once, as the panels are not blocked translationally by their higher neighbours. This means panels could also be removed from the middle of a structure, which while it may be of some benefit to assembly, would in-

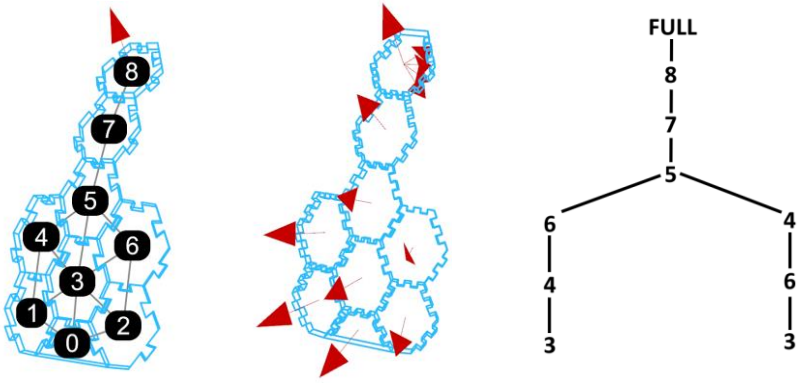

Fig. 6: Left, Centre) The results of the assembly sequencing/free direction testing for test structure of 9 panels. On the left, the dovetail joint system has only 1 panel which isn't completely constrained (the top panel #8), whilst on the right, each panel has at least 1 direction of translational freedom. **Right**) The graph of possible disassembly sequences for the dovetail set.

crease risk for sliding mode failure.

3.4 The effect of scale and adding neighbours on modelling

A larger scale test set was manufactured (Fig. 7) and had the deflection at the tip both measured and predicted, with a design height at tip of 450mm. Tests were carried out with increasing numbers of neighbours supporting the central arch (Table 3).

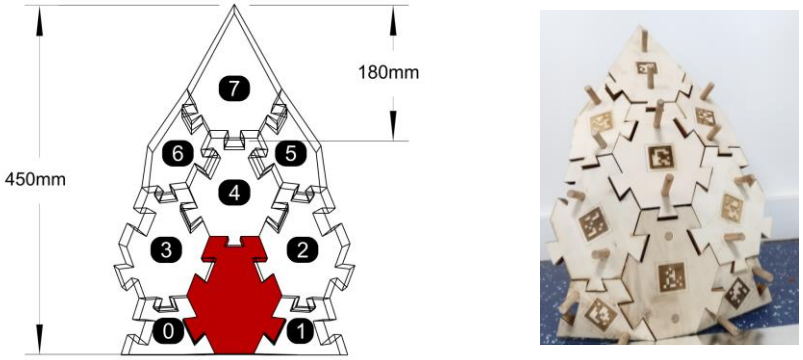

Fig. 7: A larger scale test set of panels, manufactured using a laser cutter and stacking of layers to approximate design. Panel numbers for testing are shown.

Table 3. Tip heights and estimation error

Panels present	Predicted tip height (mm) h_p	Measured tip height (mm) h_m	Difference (mm) $h_m - h_p$	% Error $\frac{h_m - h_p}{h_m}$	% difference design to measured $\frac{h_m - h_d}{h_d}$
0, 1, 4, 7	443	415	-28	-7%	-8%
0-4, 7	444	433	-11	-3%	-4%
All	446	439	-7	-2%	-2%

4 Discussion

The loft fitting process produces an approximation of an order higher than the comparison between the base and catenary. The biggest source of change in the process is the planarization, and it could be worth comparing to the form-finding integral planarization technique of Contestabile [8], planarizing whilst applying form-finding instead of post-planarizing, to see if this provides a closer solution. Additionally, comparisons could be made to ensure funicularity, through a method such as relaxed funicularity [12].

The CRA method appears to provide a reasonable level of accuracy in the estimation of deflection for the styles of discrete panel shells studied, under the assumption that panels are suitably rigid. The effect of scaling appears to introduce more error, with the predicted deflection remaining the same despite the number of supporting elements and there are some speculations as to why. First, the error is more prominent in systems with less stiffening elements ensuring rigidity, and possibly the additional panels are aiding by providing greater friction to act against self-weight. Second, it is possibly an issue with the CRA implementation, and this will require further investigation.

The dovetail style joint is shown to be far better at holding temporary bending moment forces in the structure during assembly than finger joints, albeit with a large amount of sag within the structure that increases with longer cantilevers. Alternative designs might improve this sag, both of alternative parameters and styles.

Assembly sequences are shown to be a direct effect of the joint directions, and this makes implicit sense as the joint directions are driven by the liaison graph.

5 Conclusions

In this work, it has been shown that CRA is promising for the modelling of stability and deflection in discrete panel shell systems. It can be utilised for the analysis of assembly stages to look for early feedback on designing systems with reduced formwork requirements. The authors have demonstrated the potential for design of dry stacked dicrete shell structures why may self-support during assembly.

In future work, data will be presented demonstrating the effect of joint parameter variation on performance alongside the effect of varying tolerance. A further investigation will be made on applying joints which will work in positive, negative and zero

Gaussian curvature regions, to work with a larger set of shells including hypars. Further investigation into the variables effecting the CRA method potentially also need to be made to ensure that it is generally suitable as a tool for local stability and deflection checking.

Research is ongoing into the use of the tools used here for design of shells for robotic assembly; future works will additionally demonstrate the manufacture design and assembly process for larger scale shell designs.

References

1. Kao GT-C, Iannuzzo A, Thomaszewski B, Coros S, . . . Block P (2022) Coupled Rigid-Block Analysis: Stability-Aware Design of Complex Discrete-Element Assemblies. Computer-Aided Design 146:103216
2. Frick U, Mele TV, Block P (2015) Decomposing Three-Dimensional Shapes into Self-Supporting, Discrete-Element Assemblies. In: Thomsen MR, Tamke M, Gengnagel C, Faircloth B, Scheurer F (eds) Modelling Behaviour: Design Modelling Symposium 2015. Springer International Publishing, Cham, p 187-201
3. Kao GT-C (2022) COMPAS CRA: Coupled Rigid-Block Analysis (CRA) for the COMPAS framework. URL: https://blockresearchgroup.github.io/compas_cra
4. Rutten D (2007) Grasshopper 3D. URL: https://www.grasshopper3d.com/
5. Wilson R (1992) On geometric assembly planning. In: Department of Computer Science. Stanford University, Stanford University
6. Wilcock S, Boyle J, Dogar M, Iuorio O (2022) Automated robotics agents for assembly-aware design of shells. In: Hvejsel MF, Cruz PJS (eds) Fifth International Conference on Structures and Architecture. CRC Press, Aalborg, Denmark, p 1061-1068
7. Van Mele T, Popescu M, Augustynowicz E, Echenagucia TM (2016) The Armadillo Vault Computational Design and Digital Fabrication of a Freeform Stone Shell. In: Advances in Architectural Geometry 2016. vdf Hochschulverlag AG an der ETH Zürich, Zurich, Switzerland, p 344-363
8. Iuorio O, Korkis E, Contestabile M (2019) Digital Tessellation and Fabrication of the ECHO shell. In: Proceedings of IASS Annual Symposia. 60th Anniversary Symposium of the International Association for Shell and Spatial Structures Structural Membranes 2019. International Association for Shell and Spatial Structures (IASS), Barcelona, Spain
9. Jiménez P (2013) Survey on assembly sequencing: a combinatorial and geometrical perspective. Journal of Intelligent Manufacturing 24:235-250
10. Rezaei Rad A, Burton H, Rogeau N, Vestartas P, Weinand Y (2021) A framework to automate the design of digitally-fabricated timber plate structures. Computers & Structures 244:106456
11. Lee S (1993) Backward assembly planning with assembly cost analysis. In: Proceedings 1992 IEEE International Conference on Robotics and Automation. IEEE Comput. Soc. Press
12. Gabriele S, Varano V, Tomasello G, Alfonsi D (2018) R-Funicularity of form found shell structures. Engineering Structures 157:157-169